Chemistry and Biochemistry Publications   Department of Chemistry and Biochemistry

1-1-2019

Vitamin E-inspired multi-scale imaging agent

Mikel Ghelfi
Brock University

Lucas A. Maddalena
Brock University

Jeffrey A. Stuart
Brock University

Jeffrey Atkinson
Brock University

Thad A. Harroun
Brock University

See next page for additional authors

Follow this and additional works at: https://scholar.uwindsor.ca/chemistrybiochemistrypub

Part of the Biochemistry, Biophysics, and Structural Biology Commons, and the Chemistry Commons

Recommended Citation

Authors

Mikel Ghelfi, Lucas A. Maddalena, Jeffrey A. Stuart, Jeffrey Atkinson, Thad A. Harroun, and Drew Marquardt

Vitamin E-inspired Multi-scale imaging agent

Mikel Ghelfi,[†] Lucas A. Maddalena,[‡] Jeffrey A.Stuart,[‡] Jeffrey Atkinson,[†] Thad A. Harroun,[¶] and Drew Marquardt[*,§]

[†]*Department of Chemistry, Brock University, St. Catharines, Ontario, Canada*

[‡]*Department of Biological Sciences, Brock University, St. Catharines, Ontario, Canada*

[¶]*Department of Physics, Brock University, St. Catharines, Ontario, Canada*

[§]*Department of Chemistry and Biochemistry, University of Windsor, Windsor, Ontario, Canada*

E-mail: drew.marquardt@uwindsor.ca

Abstract

The production and use of multi-modal imaging agents is on the rise. The vast majority of these imaging agents are limited to a single length for the agent, which is typically at the organ or tissue scale. This work explores the synthesis of such an imaging agent and discusses the applications of our vitamin E-inspired multi-modal and multi-length scale imaging agents TB-Toc ((S,E)-5,5-difluoro-7-(2-(5-((6-hydroxy-2,5,7,8-tetramethylchroman-2-yl)methyl)thiophen-2-yl)vinyl)-9-methyl-5H-dipyrrolo-[1,2-c:2',1'-f][1,3,2]diazaborinin-4-ium-5-uide))). We investigate the toxicity of TB-Toc along with the starting materials and lipid based delivery vehicle in mouse myoblasts and fibroblasts. Further we investigate the uptake of TB-Toc delivered to cultured cells in both solvent and liposomes. TB-Toc has low toxicity, and no change in cell viability was observed up to concentrations of 10 mM. TB-Toc shows time-dependent cellular uptake that is complete in about 30 minutes. This work is the first step in realizing our vitamin E derivatives as viable multi-modal and length scale diagnostic tools.

1

Introduction

Multi-modal imagining is a sound diagnostic strategy with clinical applications in oncology, cardiology and neuropsychiatry.[1] Such imaging combines the strengths of the different modalities into the same tissue of interest, providing additional contrast to quantify or localize the site of disease. The vast majority of these multi-modal strategies combine standard medical imaging techniques such as computed tomography (CT), magnetic resonance (MR) and positron emission tomography (PET). Imaging agents that can be used across multiple modalities at the same time can simplify pharmacological aspects of administering image enhancing compounds, while providing anatomical as well as functional information. However, these well studied multi-modal strategies (PET, CT, MR) and their associated imaging agents always provide images at similar length scales and resolutions.

Recently, efforts have been made in the area of multi-scale imaging agents (MIA).[2–5] Multi-scale imaging provides separate images at different length scales; from the molecular or cellular level, to the organ or whole organism level (Figure 1). Multi-scale imaging of living systems has implications in all areas of medicine, such as mechanistic *in vivo* research, biomarker discovery, early diagnosis and personalized medicine. The purpose of a multi-scale imaging agent is thus to provide qualitative functional and localized information from the organ level down to the cellular level. Light microscopy can be used to track the cellular effects of a treatment or disease, while conventional medical imaging can reveal the organism or tissue level context for the changes seen at the cellular level. Typically, light microscopy cannot happen *in situ*, and specimen collection for separate analysis is required. Thus, to ensure that the same biological context is being imaged at both length scales, the same molecule must provide the image contrast at both length scales simultaneously. For example, a molecule may be a beta particle emitter (for PET imaging) and fluorescent (for microscopy imaging) at the same time.

Advances in cancer diagnosis and treatment are being led by improvements in MIAs that enhance the ability to track diseases through pictures generated with injected radioactive
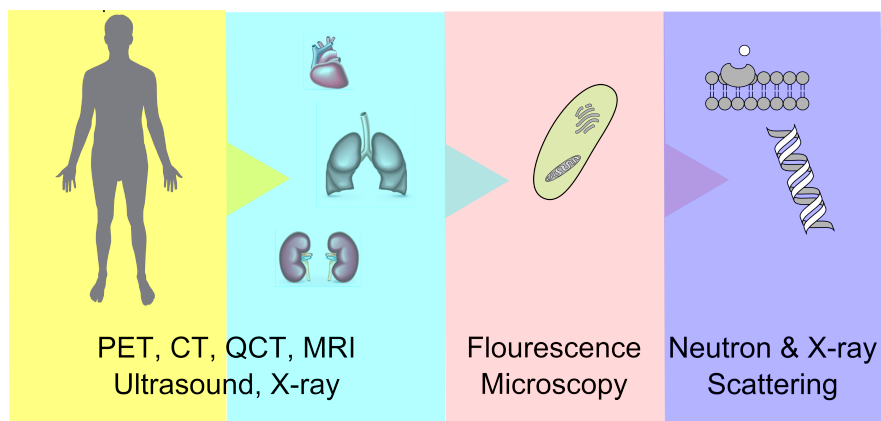
Figure 1: **Multiscale imaging.**

biomarkers. Advancements in molecular imaging, with positron emission tomography (PET) leading the way, provide clinicians with improved diagnostic power.

The usefulness of a radiotracer in cancer diagnosis is limited by a number of factors, including how well it is taken up by the body and the tumor, diagnostic reproducibility and specificity (no false positives or negatives), and overall safety. Currently, 96% of PET imaging is performed using just one compound, fludeoxyglucose (FDG), which targets cancer in a non-specific manner. FDG has limitations in detecting certain types of tumors and can accumulate in otherwise healthy areas of the body where it contributes to false positives and delivers a significant radioactive dose to the patient. Despite these limitations, the usefulness of PET is best demonstrated by current data suggesting that in as many as one-third to one-half of cancer cases, physicians who do not have access to PET may be choosing the wrong management or treatment strategy for their patients.[6–8] A recent Canadian study found that the information derived from PET imaging resulted in a change in intended treatment plans in 50% of cases.[9]

Thus, there has been a tremendous amount of research on PET radio-tracers that can improve on FDG. Take-up of newly designed radio-tracers by different tissues can be quickly quantified by screening radioactivity levels, however we argue that in the rational design of such molecules a better approach is to understand the reasons for take-up or rejection by cancer cells versus healthy cells. For example, live cell fluorescence microscopy can be

employed to visualize the incorporation of a candidate molecule into normal or cancer cells. However, this requires that the radio-tracers to be fluorescent so they can be visualized optically at such small length scales.

The use of fluorescence microscopy to observe absorption and intracellular transportation of a labeled molecule can be achieved with photo-stable fluorescent probes. In particular, probes with a fluorophore that absorbs at wavelengths greater than ~500 nm makes for better light penetration in cells and tissues within a patient. Furthermore, the fluorophore should be photo-stable during the course of this irradiation – a well-known property of the BODIPY family of compounds.[10] BODIPY dyes are notable for their uniquely small Stokes shift, high environment-independent fluorescence quantum yields, and sharp excitation and emission peaks contributing to overall brightness. Many bio-molecules have been successfully labeled with BODIPY moieties for countless research purposes.

Based on our past experience with tocopherol chemistry, we are now exploring the development of a family of multi-scale imaging compounds related to the vitamin E family combining F-18 PET radio-agent and BODIPY fluorescence. α-Tocopherol (αToc) is the predominant member of the tocopherol family taken up by the human body. We have generated a F-18 BODPY labeled derivative, thienyl-ene-BODIPY-α-tocopherol (TB-Toc).[11] In this paper, we test whether such significant chemical alterations of αToc alters its effective cellular uptake and low-toxicity. Furthermore, since αToc is a lipid and not water soluble, the molecule is most effectively delivered by liposomal formulation. This opens up the possibility of antibody-guided targeting to specific cell types. We therefore also test TB-Toc's take-up and toxicity when delivered via liposome. Since αToc has few known receptors with the exception, for example, of the a-tocopherol transfer protein, we hypothesize that the cellular toxicity of TB-Toc will remain very low, with high take-up that allows for quality fluorescent images.

For comparison's sake, we include two non-fluorescent intermediate compounds, modified at the αToc headgroup. These compounds are (2R)-2,5,7,8-tetramethyl-2-(4,8,12-trimethyltridecyl)chroman

(H-toc) and (2R)-6-iodo-2,5,7,8-tetramethyl-2-(4,8,12-trimethyltridecyl)chroman (I-toc) which could be present in trace amounts in the clinical production and use of F-toc.

Results

Since future development of the molecules described here will employ live mouse models, we focused on two murine cell lines, C2C12 mouse myoblasts and mouse embryonic fibroblasts (MEFs). The two cell lines were cultured in the presence of each of the tocopherol derivatives shown in Fig. 2 and a LUV-based delivery vehicle. In addition, the cellular uptake of the TB-Toc derivative was studied to demonstrate the multiscale imaging capabilities of TB-Toc.

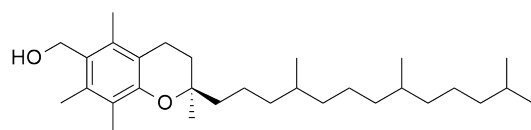## Viability of mouse cells cultured in the presence of tocopherol derivatives

We monitored viability of C2C12 and MEFs in the presence of tocopherol derivatives (Fig. 3**A** and their synthetic precursors (Fig. 3**B**) at concentrations spanning five orders of magnitude. The data in Figure 3 clearly show no sensitivity to tocopherol, 6-fluoro-tocopherol, or the hydroxymethyl tocopherol (structures shown in Fig. 2) in either the C2C12 myoblasts or the MEFs.

Furthermore, there was no evidence that either H-toc or I-toc were toxic at concentrations up to 1mM. Interestingly, the data show a clear increase in absorption at 570 nm for both myoblasts, suggesting a positive impact on the cell line.

Like the other tocopherol derivatives, TB-Toc was introduced to cell cultures of mouse myoblasts and fibroblasts at concentrations ranging over five orders of magnitude (Fig. 4B & C). Interestingly, the cultured myoblasts respond to the presence of TB-Toc. Unlike the other examined tocopherol derivatives, the TB-Toc did begin to show some loss of live myoblasts around 10-100 μM. It should be noted that 0.1 mM BODIPY-toc partially precipitated out of solution when added to culture media; it completely precipitated out of solution at 1 mM
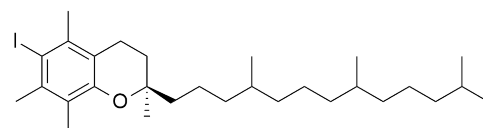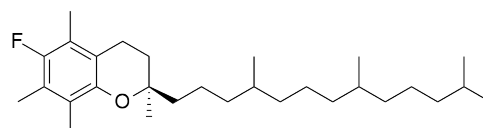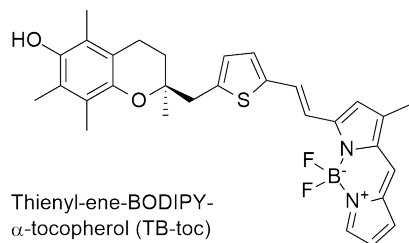
Figure 2: Structure of tocopherol, intermediates and derivatives.
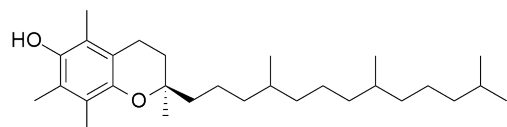
α-tocopherol (aToc)

HM-toc
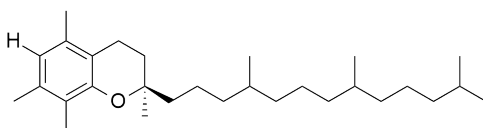
H-toc

I-toc

F-toc

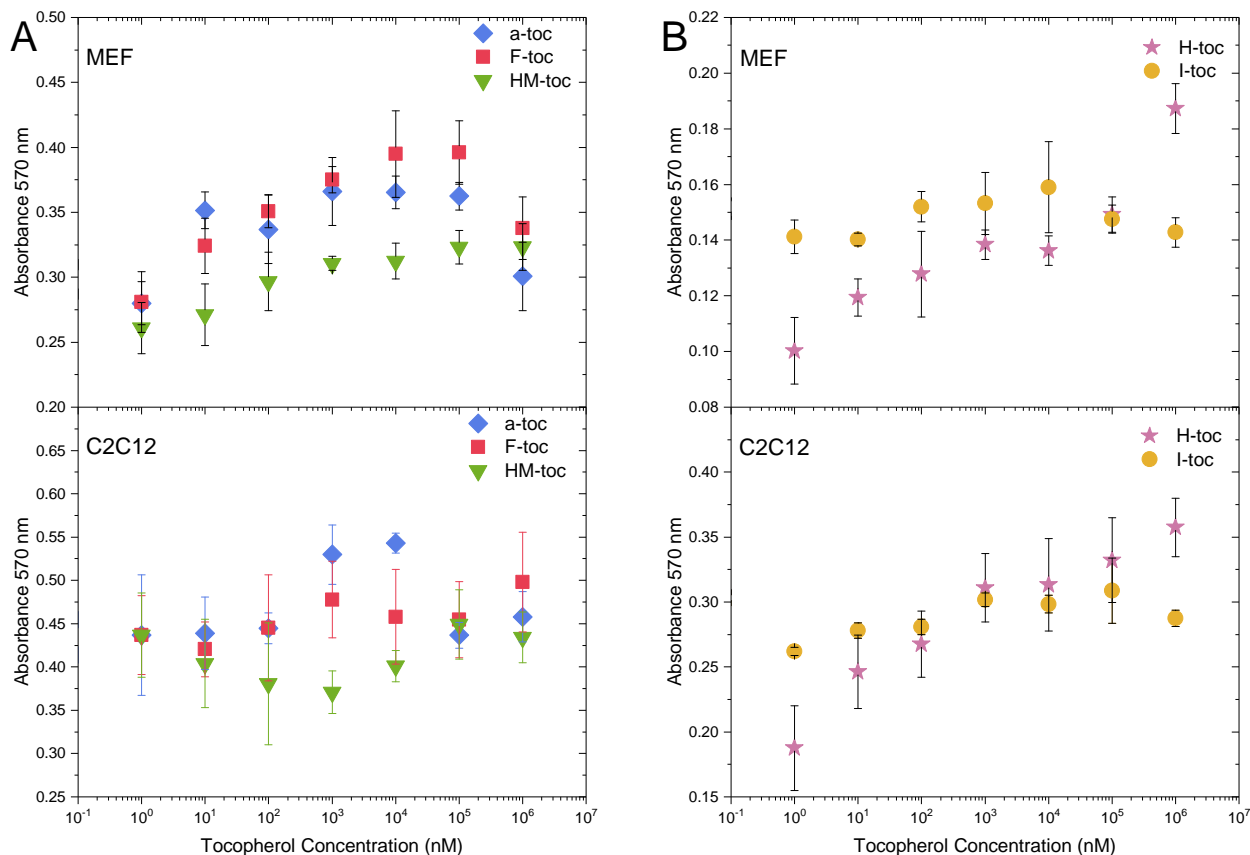Thienyl-ene-BODIPY-
α-tocopherol (TB-toc)

Figure 3: **Viability of mouse cells cultured in the presence of tocopherol derivatives at concentrations ranging from 1 nM to 1 mM.** C2C12 mouse myoblasts and mouse embryonic fibroblasts (MEFs) were treated with tocopherol derivatives (**A**) α-, F-, or HM-tocopherol and (**B**) F-toc precursor molecules I- or H-tocopherol for 24h prior to assessing viability via spectrophotometric measurement of formazan (absorbance at 570 nm) produced from the live-cell-catalyzed reduction of MTT tetrazolium (i.e. MTT viability assay). There were no significant differences between absorbance values of all tocopherol groups compared to the corresponding vehicle control (0.1% DMSO; ANOVA followed by Tukey's post-hoc test). Data points represent means $\pm$ SEM, with n = 4 for all conditions except for F-toc in MEFs (n = 3). Note: absorbance values for α-, F- and HM-toc vehicle control groups in C2C12 cells and MEFs were 0.4343 $\pm$ 0.0299 and 0.2984 $\pm$ 0.0154, respectively. Absorbance values for vehicle control groups for I- and H-toc in C2C12 cells and MEFs were 0.303 $\pm$ 0.002 and 0.151 $\pm$ 0.004, respectively.

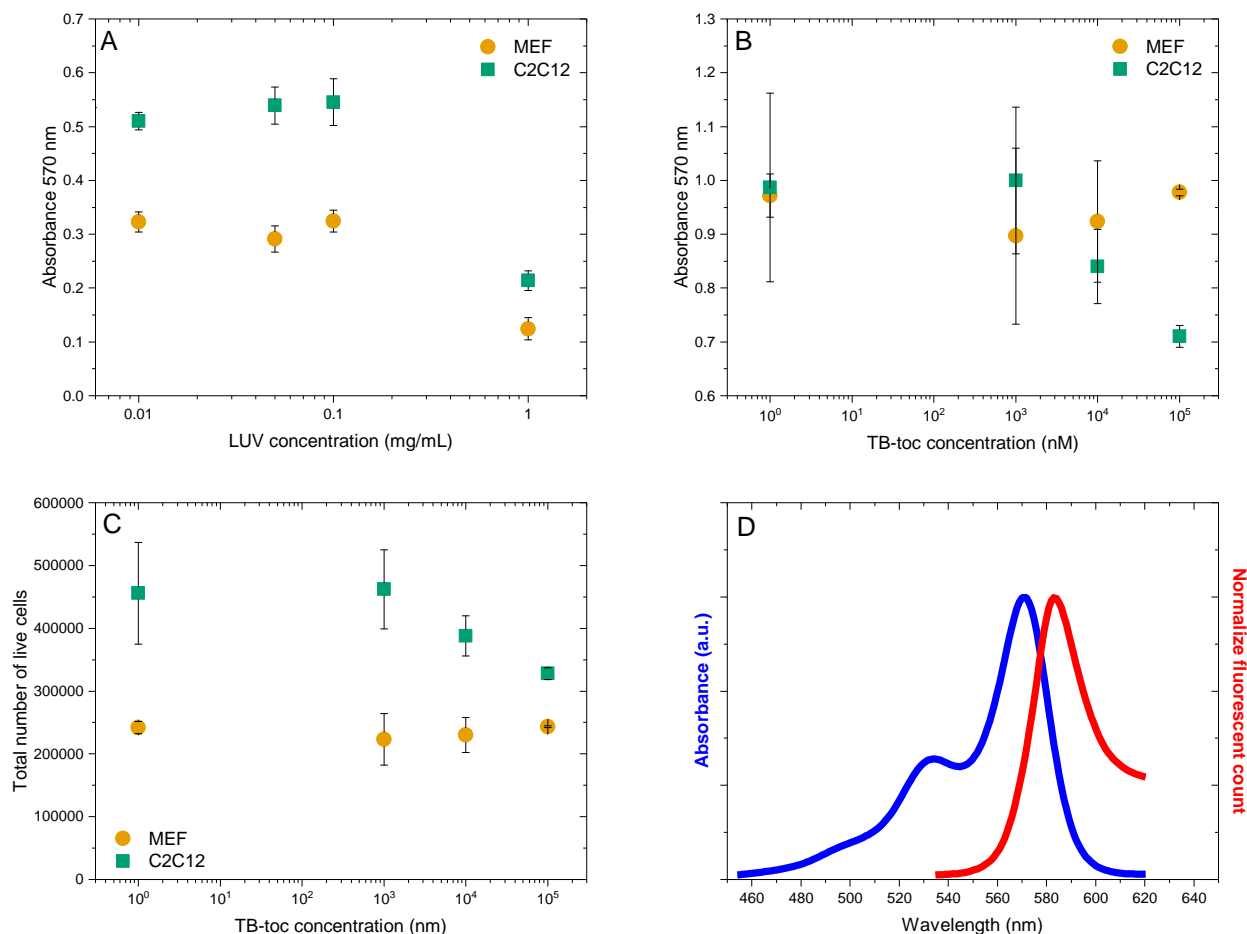and was therefore not tested at this concentration.

Figure 4: **Viability of mouse cells cultured in the presence of LUVs and BODIPY-tocopherol.** C2C12 mouse myoblasts and MEFs were treated with LUVs (**A**) and BODIPY-tocopherol (**B**) prior to assessing viability via spectrophotometric measurement of formazan (absorbance at 570 nm) produced from the live-cell-catalyzed reduction of MTT tetrazolium. Data points represent means $\pm$ SEM (LUV: n = 8; TB-Toc: n = 2). (**C**) C2C12 and MEFs were treated with BODIPY-tocopherol for 24h before determining the number of cells excluding Trypan blue dye. Data points represent means $\pm$ SEM (n = 2). The number of viable cells in the vehicle control groups for C2C12 cells and MEFs were 424,875 $\pm$ 31,125 and 249,000 $\pm$ 3,000 respectively.(**D**) TB-Toc absorption and emission spectra. Data reproduced from Ghelfi *et al.*[11]

Viability of mouse cells cultured in the presence of LUVs

We prepared LUVs composed of POPC:POPG:Cholesterol:αToc (7:3:4:0.1) sized by extrusion of the hydrated lipid suspension through a 50 nm (diameter) pore. The effective hydro-

dynamic radius of LUVs prepared in this manner was measured to be 81.9 nm as determined by dynamic light scattering. This lipid composition is already applied to the clinically used liposome-Doxorubicin suspensions.[12] However, this composition lends itself to the expeditious and simple incorporation. Specifically, the incorporation of the charged POPG which makes extrusion of 50 nm easier, and avoids the presence of plauci-lamellar species (vesicles composed of 2-3 bilayers).[13] We monitored effects of LUVs on cell viability in both the C2C12 cells and MEFs (Fig. 5) at concentrations spanning 3 orders of magnitude. The data demonstrate that the LUVs are non-toxic up to 1 mg/mL and we can safely utilize the LUVs at up to 0.1 mg/mL in both cell lines tested. Previous studies used 1 mg/mL of phospholipids[14] and 3 mM, which is approximately 2 mg/mL,[15] in similar tests with cultured Chinese hamster v79 cells and amoebae, respectively. In both cases, the concentrations examined did not appear to harm the cells.

TBtoc Uptake

The newly synthesized MIA, TB-Toc,[11] has a peak absorption at 571 nm with a smaller peak at 530 nm and the emission spectra has a maximum fluorescence wavelength of 583 nm.[11] We utilized the fluorescence properties of TB-Toc to monitor its uptake into cells.

TB-Toc was delivered to the cells using two methods, in DMSO stock solutions or in LUVs. TB-Toc was introduced to the cultures at approximately the same concentration of our MIA. Figure 5 illustrates the time-depended uptake of TB-Toc delivered to MEFs via LUVs. The data show that TB-Toc uptake is completed in approximately 30 minutes, with no observable distress to the cells. Similar results were observed for DMSO delivered TB-Toc (SI), where uptake was complete in 30 minutes. However, LUV delivery yields faster initial uptake, compared to DMSO, demonstrated by the analysis of overall intensity at each time point (Fig. 5**C**). The observation that LUV delivery yields faster initial uptake, compared to DMSO, is further visualized by the overall intensity of the images at 5 minutes after delivery (see SI).
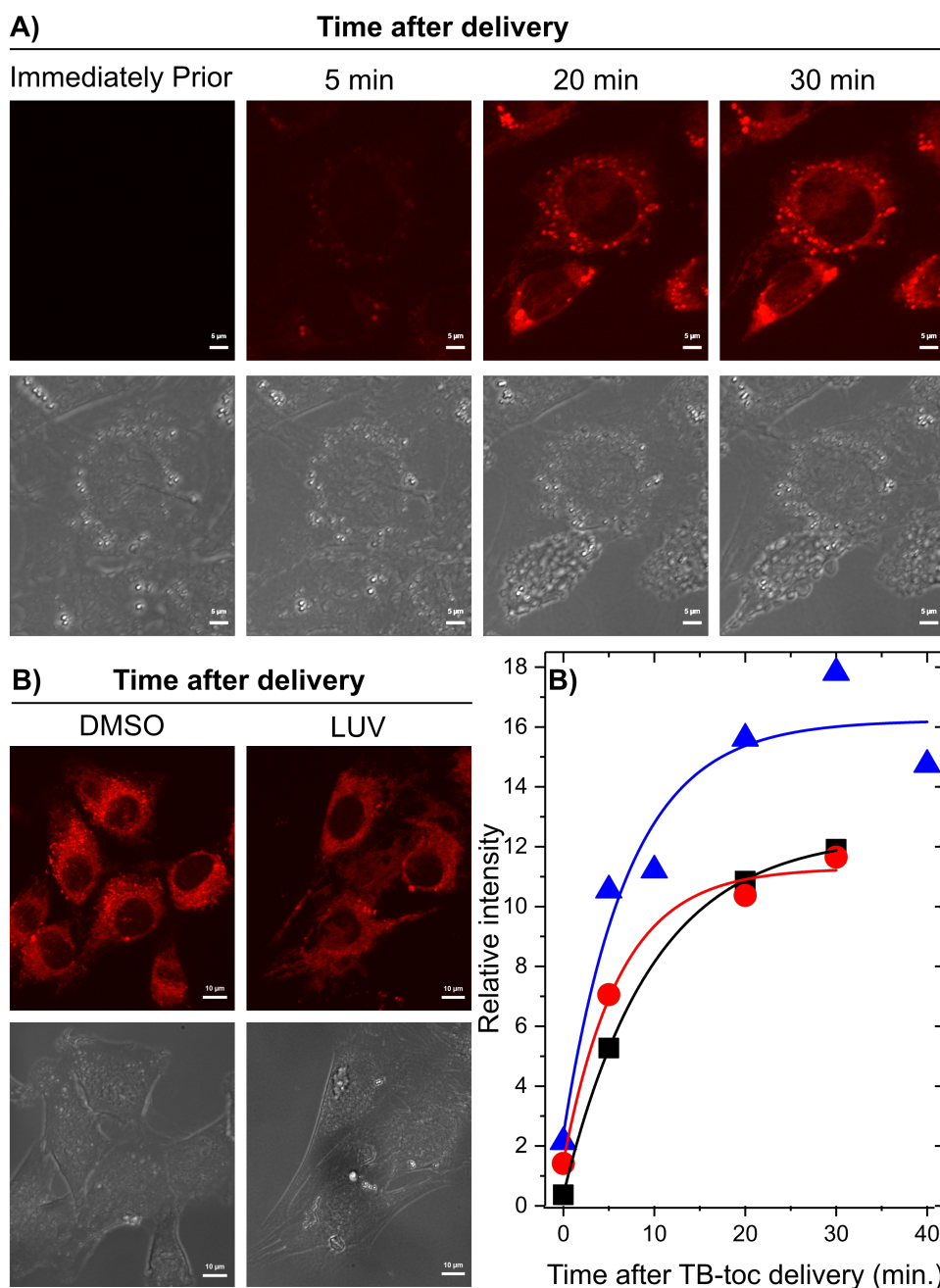
Figure 5: **Cellular uptake of BODIPY-tocopherol.** (**A**) MEF uptake of TB-Toc delivered with LUVs. Top row are fluorescence images (Ex. 587 nm; Em. 610 nm); the bottom row are the brightfield images. (**B**) Fluorescence intensity of TB-Toc in C2C12 cells delivered via DMSO and LUVs after 40 min. of incubation. Images are maximum projections of z-stacks taken at 0.32 nm intervals. (**C**) The relative fluorescence intensity of TB-Toc introduced to MEF cells via LUVs (red circles) and DMSO (black squares) and introduced to C2C12 cells via LUVs (blue triangles).

The overall intensity of the LUV delivered label is fainter than the DMSO solution, Fig. 5 **B**. However, the images suggest that delivery via DMSO and LUVs yield the same cellular distribution of TB-Toc. We suspect the brightest spots are lipid droplets, however, without co-localization studies this cannot be confirmed. Nevertheless, our data clearly demonstrate substantial cellular uptake of our MIA.

Discussion

Currently, the majority of PET imaging is performed using FDG (18F-fluorodeoxyglucose), a glucose analogue attached to a PET radiotracer (Fluorine-18). FDG targets cancer in a non-specific manner relying on the enhanced rate of glucose metabolism in fast-growing tumour cells and the slow metabolism of the deoxyglucose. The ability to incorporate 18F radio tracers onto F-toc and TB-Toc provide a new opportunity for the area of PET imaging.

Our data support the application of F-toc as a PET imagining agent. Neither the F-toc nor the tocopherol-based precursors show cytotoxicity up to a concentration of 1 mM, suggesting excellent tolerance by mammalian cells. In addition, these new molecules are relatively easy to synthesize: the two synthetic pathways to produce F-toc, either by electrophilic fluorination or nucleophilic fluorination, can be completed in under 15 minutes (see Methods and Materials). This expedient synthesis addresses the technical issues of optimized and expedient production of the F-18 labeled agent since F-18 has a short half-life of 109 minutes.

The toxicity of our TB-Toc seems to be qualitatively comparable to BODIPY-cholesterol. Although we were not able to find quantitative toxicity data for BODIPY-cholesterol in cell lines, many have reported that cells and organisms remain undisturbed with no significant delay in cell growth when incubated with BODIPY-cholesterol.[16,17]

Our presented LUV composition lacks the targeted specificity that many existing liposomal technologies offer, however it does avoid complications caused by incorporating a

polyethylene glycol coating, namely foot-mouth syndrome.[18] However, the presented tocopherol-inspired molecules toned not be delivered in the LUV composition chosen in this work. The absorption and distribution of tocopherol is well understood,[19–22] and the vast majority of tocopherol exists in cell membranes. Thus, targeted delivery of tocopherol and its derivatives using liposomal delivery vehicles should allow targeting of the new MIA to specific cell and tissue types utilizing the plethora of existing targeted liposome systems,[23–25] some of which are already clinically approved targeted lipid-based delivery technologies.[25]

Alternatively, delivery of tocopherol inspired agents without the use of a targeted LUV carrier will also prove clinically useful. The known ability of the probe to bind with high affinity to the α-tocopherol transfer protein (α-TTP) assures that the probe will be taken up with specificity by the liver, where α-TTP is abundant. The imaging of liver is particularly important at present given the growing prevalence of non-alcoholic fatty liver (NAFL) and non-alcoholic steatohepatitis (NASH), pathologies common in obese and diabetic patients. Available diagnostic and prognostic tools for NAFL are very poor, both in terms of clinical timing, sensitivity and selectivity on disease mechanisms.[26,27] Studies have demonstrated the potential for vitamin E in the prevention of NASH, such clinical guidelines are now recommending vitamin E as a first line therapy for non-diabetic adults with biopsy-proven NASH.[28–30]

Although much emphasis has been placed on the PET applications of our imaging agents, precedence has been set for the use of liposomes as diagnostic agents using the SPECT technique as PET and SPECT go hand in hand with cost and benefit.[31,32] Some of our precursor molecules, namely I-toc, could be used as a SPECT agent. The isotope ^{125}I has been used to synthesize β-, γ- and δ- tocopherols in the past.[33] However, ^{123}I is more common in imaging since it has a shorter half life (13.22h h) than [125]I (60 days) or [131]I (8 days), but all three isotopes would be viable candidates for a SPECT agent and the optimal isotope depends on the application.

There have not been many SPECT agents to monitor liposomal delivery via the lipo-

somal membrane, rather, they use Technecium-99m, Indium-111.[34] Metals have there own toxicological issues, are much more unnatural to the body than iodide (iodine is in thyroid glands, etc.) and need chelating agents to be bound to the liposome. We have demonstrated that our I-toc is not toxic. If the I-toc were to degrade by oxidation, it would form I^- and tocopherol and/or tocopherol-quinone. Since αToc is often added to protect liposomal delivery systems,[12] the I-toc would be relatively safe from degradation. Further, SPECT and PET can be imaged at the same time; thus, a liposome mixture of 18F-toc and I-toc could allow for SPECT/PET images to be collected simultaneously.[35]

Conclusion

The present work presents a molecule that has the desired properties of an imaging fluorophore while also serving as a PET agent. Furthermore the technology can be used for both purposes simultaneously. The dual-modality probe (PET and fluorescence) presented in this work are designed to be hydrophobic, thus, compatible with liposome based antibody-directed imaging techniques.[23–25]

Methods and Materials

Materials

C2C12 mouse myoblasts, Dulbecco's Modified Eagle Medium (DMEM; with high glucose, L-glutamine, sodium pyruvate, and sodium bicarbonate), Eagle's minimum essential medium (MEM) non-essential amino acids solution, penicillin/streptomycin solution, fetal bovine serum (FBS), and thiazolyl blue tetrazolium bromide (MTT) were purchased from Sigma-Aldrich (St. Louis, MO). Mouse embryonic fibroblasts (MEFs) were purchased from ATCC (Manassas, VA). 96-well cell culture microplates (polystyrene, clear flat-bottom) were purchased from Greiner Bio-One (Frickenhausen, Germany). 6-well cell culture plates were

purchased from Sarstedt (Newton, SC). Dimethyl sulfoxide (DMSO) was purchased from Bio-Shop (Burlington, ON, Canada).1-palmitoyl-2-oleoyl-sn-glycero-3-phosphocholine (16:0/18:1 PC, POPC), 1-palmitoyl-2-oleoyl-sn-glycero-3-phosphocholine [16:0/18:1 PC, POPC], and 1-palmitoyl-2-oleoyl-sn-glycero-3-phospho-(1'-rac-glycerol) (sodium salt) [16:0/18:1 PG, POPG] were purchased from Avanti Polar Lipids (Alabaster, AL) and used as received. Unless otherwise indicated, all other materials were purchased from Sigma-Aldrich (St. Louis, MO, USA), BioShop (Burlington, ON, Canada), or Fisher Scientific (Mississauga, ON, Canada).

Synthesis of F-Toc by electrophilic fluorination

H-Toc (1eq) was mixed with N-fluorobenzenesulfonimide (1eq) and stirred in dry acetonitrile as a 1M solution for 10-15min at 150°C. The reaction was cooled to room temperature, extracted with CH_2Cl_2 and water, the organic phase dried over Na_2SO_4 and evaporated down to dryness. The crude product was filtrated trough a silica plug with hexane to remove polar byproducts. Silica column chromatography (gradient Hexane to Hexane/CH_2Cl_2 99:1) afforded F-Toc (44%) as a clear oil.
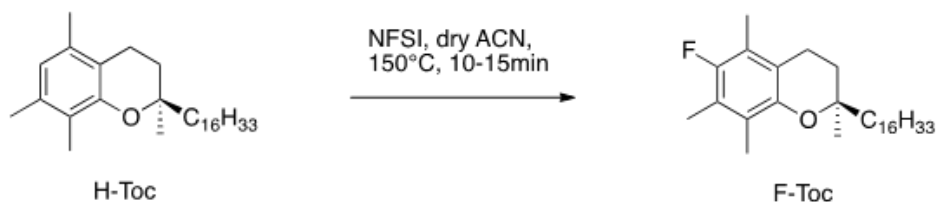
To a 0.85M solution of I-Toc (1eq) in dry THF at 0°C under an N2 atmosphere was a 1.7M t-BuLi solution in pentane (2eq) added and stirred for 1min. An 0.35M N-fluorobenzenesulfonimide (2eq) solution in THF was slowly added and stirred for 1min at 0°C. The reaction was quenched with methanol, the solvents evaporated, extracted with CH_2Cl_2 and water, the organic phase dried over Na_2SO_4 and evaporated down to dryness. Silica column chromatography (gradient Hexane to Hexane/CH_2Cl_2 99:1) afforded F-Toc (15%) as a clear oil. This strategy was adapted from previously reported methods.[36,37]
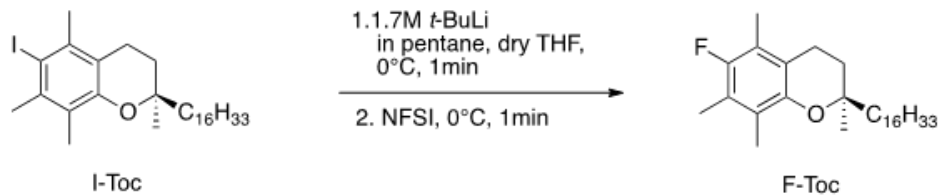
Synthesis of F-Toc by nucleophilic fluorination

(Phenyl)tocopherol iodonium tosylate prepared by previously reported methods (1eq),[38] was dissolved in DMF as a 5mM solution, 1M tetrabutylammonium fluoride in THF (1M TBAF in THF, 1eq) was added and stirred for 15min at 150°C. The solvent was evaporated to dryness and the residual mixture partitioned between hexane and water. The organic phase was dried with Na_2SO_4, filtrated and purified over a small SiO2 column with hexane. Silica column chromatography (gradient Hexane to Hexane/CH_2Cl_2 99:1) afforded F-Toc (24%) as a clear oil.This synthetic strategy was adapted from previously reported methods.[39]
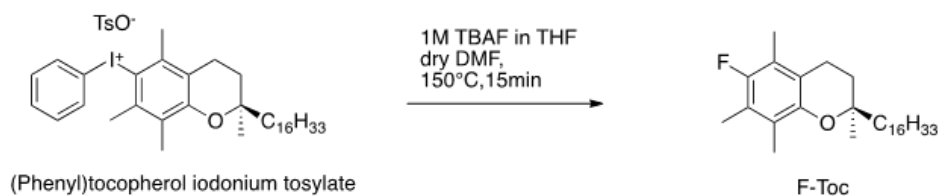

TLC: Rf = 0.27 (Hexane) **^{1}H-NMR (400MHz, CDCl3):** δ 2.60 (t, J = 6.80 Hz, 2H, ArCH2CH2), δ 2.16 (d, J = 6.80 Hz, 3H, ArCH3), δ 2.12 (d J = 1.60 Hz, 3H, ArCH3), δ 2.11 (s, 3H, ArCH3), δ 1.81 (enant. dt, J = 6.80 Hz, 2H, ArCH2CH2), δ 1.65-1.04 (m, 21H, phytyl-CH/CH2 + 2'R-CH3) δ 8.88 (m, 12H, phytyl-CH3)

^{13}C-NMR (100MHz, CDCl3): 154.45, 152.13, 147.07, 147.06, 123.10, 123.06, 121.41, 121.22, 119.08, 118.90, 117.60, 117.56, 74.91, 39.86, 39.77, 39.38, 37.57, 37.53, 37.45, 37.40, 37.33, 37.29, 32.79, 32.69, 31.26, 31.20, 29.71, 27.99, 24.82, 24.45, 23.81, 22.73, 22.63, 21.02, 20.36, 20.34, 19.75, 19.69, 19.64, 19.60 **^{19}F-NMR (400MHz, CDCl3):** -131.49, -131.50 (d, J = 4 Hz, 1F, Ar-F) MS [EI+] m/z 432.49 (M, 10%), m/z 205.18 (100%), HRMS Calculated

for C29H51NO 429.3971; found: 432.3762

Synthesis of TB-Toc

TB-Toc was synthesized following previously reported methods.[11]

Cell Culture

C2C12 mouse myoblasts and mouse embryonic fibroblasts (MEFs) were cultured in DMEM supplemented with 10% (v/v) FBS, 4500 mg/L glucose, 4 mM L-glutamine, 1 mM sodium pyruvate, 2% (v/v) MEM nonessential amino acid solution, and penicillin (50 I.U./mL) / streptomycin (50 μg/mL) solution (complete media). Cells were cultured in a humidified 5% CO_2 atmosphere within a Thermo Forma Series II water-jacketed CO_2 incubator maintained at 37°C. Cells were transferred to fresh 96- or 6-well plates (2,000 cells/well & 60,000 cells/well, respectively) in the evening prior to commencing tocopherol treatments.

Liposome stock solutions and cell treatments

Phospholipid films were prepared by transferring the desired volumes of stock solutions of POPC:POPG:Cholesterol:αToc (or TBtoc), at a molar ratio of 7:3:4:0.1, to a glass vial. Organic solvent was then removed with an N_2 stream and gentle heating, followed by drying in vacuo ($\geq$6 h). Lipid films were hydrated with phosphate buffered saline (pH 7.4) to a concentration of 10 mg/mL. The resulting multilamellar vesicle (MLV) suspensions were incubated at 30°C and subjected to five freeze/thaw cycles. Large unilamellar vesicles (LUVs) were prepared by passing the MLV suspensions through a single use sterile 50 nm NanoSizer (T&T Scientific, Knoxville, TN) 31 times at room temperature.

Tocopherol stock solutions and cell treatments

Each tocopherol was dissolved in sterile 100% DMSO to yield a 1 M stock solution. Less concentrated stock solutions were subsequently prepared using ten-fold serial dilutions. All tocopherol solutions were stored at -20°C. To treat cultured cells, media was replaced with complete media containing freshly-added tocopherol; the final amount of vehicle (DMSO) for all concentrations tested was 0.1% (v/v).

MTT tetrazolium reduction assay

Media was discarded, wells were washed once with phenol red-free complete culture media, and 100 μL/well phenol red-free complete culture media containing 0.45 mg/mL MTT was added. Two hours later, solubilization solution [40% (v/v) dimethylformamide, 2% (v/v) glacial acetic acid, 16% (w/v) sodium dodecyl sulfate, pH 4.7] was added (100 μL/well) and well contents were gently mixed by re-suspension to dissolve the formazan precipitate. Plates were incubated at room temperature in darkness for 2h before recording absorbance at 570 nm using a Bio-Tek PowerWave Microplate UV-Vis spectrophotometer (Winooski, VT, USA). For each plate, background signal averaged from cell-free wells containing vehicle treatments was subtracted.

Trypan blue exclusion assay

Media was discarded, wells were washed once with phosphate-buffered saline, and cells were harvested via trypsinization. After centrifugation (240 g, 3 min), cell pellets were re-suspended in complete culture media and subsequently diluted in 0.4% (w/v) Trypan Blue solution. Three minutes later, the numbers of viable (non-stained) cells were counted using a hemocytometer (Hausser Scientific, Horsham, PA) viewed under a Hund Wetzlar Wilovert Inverted Phase-Contrast light microscope (Fisher Scientific, Mississauga, ON, Canada).

Live-cell fluorescence microscopy

Fluorescence imaging of live cells was performed using Zeiss Axio Observer.Z1 inverted light/epifluorescence microscope equipped with ApoTome.2 optical sectioning, a Plan-Apochromat 63x/1.40 Oil DIC M27 objective lens, and a Hamamatsu ORCA-Flash4.0 V2 digital camera. Both the intensity of fluorescence illumination achieved via an X-Cite 120LED light source and camera exposure times were held constant between experiments. BODIPY fluorescence was viewed using excitation and emission wavelength filter sets of 540 – 552 nm and 590 – 660 nm, respectively, with set excitation and emission wavelengths of 587 nm and 610 nm, respectively (Zeiss Item# 411003-0010-000). Z-stack series consisted of approximately 20 – 40 slices taken at 0.32 μm intervals and were rendered into 2D maximum intensity projections using the 'extended depth of focus' processing tool in Zeiss Zen 2 (blue edition) microscopy software. The microscope stage and objective were maintained at 37°C using a TempModule S-controlled stage heater and objective heater (PeCon, Erbach, Germany). A humidified 5% CO_2 environment was achieved via tubing connected to a humidified CO_2 culture incubator. One day prior to imaging, cells were seeded onto MatTek poly-D-lysine-coated glass bottom culture dishes in complete culture media devoid of phenol red.

Fluorescence intensity was analyzed from the microscope images using the ImageJ software.[40,41]

Statistical Analyses

Data sets were analyzed in GraphPad Prism 5 using one-way ANOVA and Turkey's post-hoc test, with a p-value of less than 0.05 considered significant.

Author contributions statement

J.A., T.A.H. and D.M. conceived the project. J.A.S., J.A., T.A.H. and D.M. conceived the experiments. M.G. and L.A.M. conducted the experiments and analyzed the results. T.A.H.

and D.M. prepared the manuscript and MG, J.A. and J.S. provided extensive editing and scientific input. All authors reviewed the manuscript.

Additional information

Acknowledgement

References

(1) Martí-Bonmatí, L.; Sopena, R.; Bartumeus, P.; Sopena, P. Multimodality imaging techniques. *Contrast Media & Molecular Imaging* **2010**, *5*, 180–189.

(2) Malik, B. H.; Jabbour, J. M.; Cheng, S.; Cuenca, R.; Cheng, Y.-S. L.; Wright, J. M.; Jo, J. A.; Maitland, K. C. A novel multimodal optical imaging system for early detection of oral cancer. *Oral surgery, oral medicine, oral pathology and oral radiology* **2016**, *121*, 290–300.e2.

(3) Fatakdawala, H.; Poti, S.; Zhou, F.; Sun, Y.; Bec, J.; Liu, J.; Yankelevich, D. R.; Tinling, S. P.; Gandour-Edwards, R. F.; Farwell, D. G.; Marcu, L. Multimodal in

vivo imaging of oral cancer using fluorescence lifetime, photoacoustic and ultrasound techniques. *Biomedical optics express* **2013**, *4*, 1724–1741.

(4) Bec, J.; Xie, H.; Yankelevich, D. R.; Zhou, F.; Sun, Y.; Ghata, N.; Aldredge, R. C.; Marcu, L. Design, construction, and validation of a rotary multifunctional intravascular diagnostic catheter combining multispectral fluorescence lifetime imaging and intravascular ultrasound. *Journal of Biomedical Optics* **2012**, *17*, 17 – 17 – 10.

(5) Sun, Y.; Xie, H.; Liu, J.; Lam, M.; Chaudhari, A. J.; Zhouand, F.; Bec, J.; Yankelevich, D. R.; Dobbie, A.; Tinling, S. P.; Gandour-Edwards, R.; Monsky, W. L.; Farwell, G. D.; Marcu, L. In vivo validation of a bimodal technique combining time-resolved fluorescence spectroscopy and ultrasonic backscatter microscopy for diagnosis of oral carcinoma. *Journal of Biomedical Optics* **2012**, *17*, 17 – 17 – 11.

(6) Hillner, B. E.; Siegel, B. A.; Shields, A. F.; Liu, D.; Gareen, I. F.; Hanna, L.; Stine, S. H.; Coleman, R. E. The impact of positron emission tomography (PET) on expected management during cancer treatment: findings of the National Oncologic PET Registry. *Cancer* **2009**, *115*, 410–418.

(7) Hillner, B. E.; Siegel, B. A.; Shields, A. F.; Liu, D.; Gareen, I. F.; Hunt, E.; Coleman, R. E. Relationship between cancer type and impact of PET and PET/CT on intended management: findings of the national oncologic PET registry. *Journal of nuclear medicine : official publication, Society of Nuclear Medicine* **2008**, *49*, 1928–1935.

(8) Hillner, B. E.; Siegel, B. A.; Liu, D.; Shields, A. F.; Gareen, I. F.; Hanna, L.; Stine, S. H.; Coleman, R. E. Impact of positron emission tomography/computed tomography and positron emission tomography (PET) alone on expected management of patients with cancer: initial results from the National Oncologic PET Registry. *Journal of clinical oncology : official journal of the American Society of Clinical Oncology* **2008**, *26*, 2155–2161.

(9) Worsley, D. F.; Wilson, D. C.; Powe, J. E.; Benard, F. Impact of F-18 Fluorodeoxyglucose Positron Emission TomographyâĂŞComputed Tomography on Oncologic Patient Management: First 2 Years' Experience at a Single Canadian Cancer Center. *Canadian Association of Radiologists Journal* **2010**, *61*, 13 – 18.

(10) Loudet, A.; Burgess, K. BODIPY Dyes and Their Derivatives: Synthesis and Spectroscopic Properties. *Chemical Reviews* **2007**, *107*.

(11) Ghelfi, M.; Ulatowski, L.; Manor, D.; Atkinson, J. Synthesis and characterization of a fluorescent probe for α-tocopherol suitable for fluorescence microscopy. *Bioorganic & Medicinal Chemistry* **2016**, *24*, 2754 – 2761.

(12) Barenholz, Y.; Gabizon, A. Liposome/doxorubicin composition and method. US Patent 4,898,735, 1990.

(13) Heberle, F. A.; Marquardt, D.; Doktorova, M.; Geier, B.; Standaert, R. F.; Heftberger, P.; Kollmitzer, B.; Nickels, J. D.; Dick, R. A.; Feigenson, G. W.; Katsaras, J.; London, E.; Pabst, G. Subnanometer Structure of an Asymmetric Model Membrane: Interleaflet Coupling Influences Domain Properties. *Langmuir* **2016**, *32*, 5195–5200.

(14) Huang, L.; Pagano, R. E. Interaction of phospholipid vesicles with cultured mammalial cells. I. Characteristics of uptake. *The Journal of cell biology* **1975**, *67*, 38–48.

(15) Batzri, S.; Korn, E. D. Interaction of phospholipid vesicles with cells. Endocytosis and fusion as alternate mechanisms for the uptake of lipid-soluble and water-soluble molecules. *The Journal of cell biology* **1975**, *66*, 621–634.

(16) Hölttä-Vuori, M.; Uronen, R.-L.; Repakova, J.; Salonen, E.; Vattulainen, I.; Panula, P.; Li, Z.; Bittman, R.; Ikonen, E. BODIPY-cholesterol: a new tool to visualize sterol trafficking in living cells and organisms. *Traffic (Copenhagen, Denmark)* **2008**, *9*, 1839–1849.

(17) Crowley, J. T.; Toledo, A. M.; LaRocca, T. J.; Coleman, J. L.; London, E.; Benach, J. L. Lipid exchange between Borrelia burgdorferi and host cells. *PLoS pathogens* **2013**, *9*, e1003109.

(18) Rafiyath, S. M.; Rasul, M.; Lee, B.; Wei, G.; Lamba, G.; Liu, D. Comparison of safety and toxicity of liposomal doxorubicin vs. conventional anthracyclines: a meta-analysis. *Experimental hematology & oncology* **2012**, *1*, 10.

(19) Atkinson, J.; Harroun, T.; Wassall, S. R.; Stillwell, W.; Katsaras, J. The location and behavior of a-tocopherol in membranes. *Molecular Nutrition & Food Research* **2010**, *54*, 641–651.

(20) Marquardt, D.; Williams, J. A.; Kučerka, N.; Atkinson, J.; Wassall, S. R.; Katsaras, J.; Harroun, T. A. Tocopherol Activity Correlates with Its Location in a Membrane: A New Perspective on the Antioxidant Vitamin E. *Journal of the American Chemical Society* **2013**, *135*, 7523–7533.

(21) Marquardt, D.; Williams, J. A.; Kinnun, J. J.; Kučerka, N.; Atkinson, J.; Wassall, S. R.; Katsaras, J.; Harroun, T. A. Dimyristoyl Phosphatidylcholine: A Remarkable Exception to α-Tocopherol's Membrane Presence. *Journal of the American Chemical Society* **2014**, *136*, 203–210.

(22) Marquardt, D.; Kučerka, N.; Katsaras, J.; Harroun, T. A. α-Tocopherol's Location in Membranes Is Not Affected by Their Composition. *Langmuir* **2015**, *31*, 4464–4472.

(23) Abulrob, A.; Stanimirovic, D.; Iqbal, U.; Nieh, M.-P.; Katsaras, J. Antibody-targeted Carrier for Contrast Agents. 2011.

(24) Iqbal, U.; Albaghdadi, H.; Nieh, M.-P.; Tuor, U. I.; Mester, Z.; Stanimirovic, D.; Katsaras, J.; Abulrob, A. Small unilamellar vesicles: a platform technology for molecular imaging of brain tumors. *Nanotechnology* **2011**, *22*, 195102.

(25) Allen, T. M.; Cullis, P. R. Liposomal drug delivery systems: From concept to clinical applications. *Advanced Drug Delivery Reviews* **2013**, *65*, 36 – 48, Advanced Drug Delivery: Perspectives and Prospects.

(26) Goceri, E.; Shah, Z. K.; Layman, R.; Jiang, X.; Gurcan, M. N. Quantification of liver fat: A comprehensive review. *Computers in biology and medicine* **2016**, *71*, 174–189.

(27) Kahl, S.; Straßburger, K.; Nowotny, B.; Livingstone, R.; Klüppelholz, B.; Keßel, K.; Hwang, J.-H.; Giani, G.; Hoffmann, B.; Pacini, G.; Gastaldelli, A.; Roden, M. Comparison of liver fat indices for the diagnosis of hepatic steatosis and insulin resistance. *PloS one* **2014**, *9*, e94059.

(28) Chalasani, N.; Younossi, Z.; Lavine, J. E.; Diehl, A. M.; Brunt, E. M.; Cusi, K.; Charlton, M.; Sanyal, A. J.; Association, A. G.; for the Study of Liver Diseases, A. A.; of Gastroenterologyh, A. C. The diagnosis and management of non-alcoholic fatty liver disease: practice guideline by the American Gastroenterological Association, American Association for the Study of Liver Diseases, and American College of Gastroenterology. *Gastroenterology* **2012**, *142*, 1592–1609.

(29) Watanabe, S. et al. Evidence-based clinical practice guidelines for nonalcoholic fatty liver disease/nonalcoholic steatohepatitis. *Hepatology research : the official journal of the Japan Society of Hepatology* **2015**, *45*, 363–377.

(30) Arab, J. P.; Candia, R.; Zapata, R.; Muñoz, C.; Arancibia, J. P.; Poniachik, J.; Soza, A.; Fuster, F.; Brahm, J.; Sanhueza, E.; Contreras, J.; Cuellar, M. C.; Arrese, M.; Riquelme, A. Management of nonalcoholic fatty liver disease: an evidence-based clinical practice review. *World journal of gastroenterology* **2014**, *20*, 12182–12201.

(31) Silindir, M.; ErdoÄ§an, S.; ÃŰzer, A. Y.; DoÄ§an, A. L.; Tuncel, M.; ÃŰmer UÄ§ur,; Torchilin, V. P. Nanosized multifunctional liposomes for tumor diagnosis and molecular imaging by SPECT/CT. *Journal of Liposome Research* **2013**, *23*, 20–27.

(32) Mitchell, N.; Kalber, T. L.; Cooper, M. S.; Sunassee, K.; Chalker, S. L.; Shaw, K. P.; Ordidge, K. L.; Badar, A.; Janes, S. M.; Blower, P. J.; Lythgoe, M. F.; Hailes, H. C.; Tabor, A. B. Incorporation of paramagnetic, fluorescent and PET/SPECT contrast agents into liposomes for multimodal imaging. *Biomaterials* **2013**, *34*, 1179 – 1192.

(33) Dewanjee, M. K. *Radioiodinated Small Molecules and Their Applications*; Developments in Nuclear Medicine; Springer, 1992; Vol. 21; Chapter 10, pp 233–387.

(34) van der Geest, T.; Laverman, P.; Metselaar, J. M.; Storm, G.; Boerman, O. C. Radionuclide imaging of liposomal drug delivery. *Expert Opinion on Drug Delivery* **2016**, *13*, 1231–1242.

(35) Stanton, S. E.; Eary, J. F.; Marzbani, E. A.; Mankoff, D.; Salazar, L. G.; Higgins, D.; Childs, J.; Reichow, J.; Dang, Y.; Disis, M. L. Concurrent SPECT/PET-CT imaging as a method for tracking adoptively transferred T-cells in vivo. *Journal for ImmunoTherapy of Cancer* **2016**, *4*, 27.

(36) Andreev, R. V.; Borodkin, G. I.; Shubin, V. G. Fluorination of aromatic compounds with N-fluorobenzenesulfonimide under solvent-free conditions. *Russian Journal of Organic Chemistry* **2009**, *45*, 1468.

(37) Aiichiro, N.; Yuki, U.; Heejin, K.; JunâĂŘichi, Y. Synthesis of Functionalized Aryl Fluorides Using Organolithium Reagents in Flow Microreactors. *Chemistry âĂŞ An Asian Journal* **2103**, *8*, 705–708.

(38) Chun, J.-H.; Pike, V. W. Regiospecific Syntheses of Functionalized Diaryliodonium Tosylates via [Hydroxy(tosyloxy)iodo]arenes Generated in Situ from (Diacetoxyiodo)arenes. *The Journal of Organic Chemistry* **2012**, *77*, 1931–1938.

(39) Chun, J.-H.; Pike, V. W. Single-step syntheses of no-carrier-added functionalized [18F]fluoroarenes as labeling synthons from diaryliodonium salts. *Org. Biomol. Chem.* **2013**, *11*, 6300–6306.

(40) Schneider, C.; Rasband, W.; Eliceiri, K. Nature Methods. *Biophotonics International* **2012**, *9*, 671–675.

(41) Abramoff, M.; Magalhaes, P.; Ram, S. Image Processing with ImageJ. *Biophotonics International* **2004**, *11*, 36–42.

Graphical TOC Entry